Supplementary Materials for:

Submonolayer Biolasers for Ultrasensitive Biomarker Detection

Chaoyang Gong[1,3,7], Xi Yang[1,2,7], Shui-Jing Tang[2,7], Qian-Qian Zhang[1,7], Yanqiong Wang[1], Yi-Ling Liu[1], Yu-Cheng Chen[3], Gang-Ding Peng[5], Xudong Fan[6], Yun-Feng Xiao[2,*], Yun-Jiang Rao[1,4,*], and Yuan Gong[1,*]

[1] Key Laboratory of Optical Fibre Sensing and Communications (Ministry of Education of China), School of Information and Communication Engineering, University of Electronic Science and Technology of China, Chengdu, Sichuan 611731, People's Republic of China.

[2] State Key Laboratory for Mesoscopic Physics and Frontiers Science Centre for Nano-optoelectronics, School of Physics, Peking University, Beijing 100871, People's Republic of China.

[3] School of Electrical and Electronic Engineering, Nanyang Technological University, Singapore 639798, Singapore.

[4] Research Centre for Optical Fibre Sensing, Zhejiang Laboratory, Hangzhou, Zhejiang 310000, People's Republic of China.

[5] School of Electrical Engineering and Telecommunications, University of New South Wales, Sydney, NSW 2052, Australia.

[6] Department of Biomedical Engineering, University of Michigan, Ann Arbor, Michigan 48109, USA.

[7] These authors contributed equally: Chaoyang Gong, Xi Yang, Shui-Jing Tang, and Qian-Qian Zhang.

*E-mails: yfxiao@pku.edu.cn; yjrao@uestc.edu.cn; ygong@uestc.edu.cn

CONTENTS

1. Surface modification

The process for the surface modification of optical fibre is illustrated in Fig. S1a, including hydroxylation, silanization, biotinylation, as well as specific conjugation between biotin and streptavidin molecules. The details are also described in Methods.

According to the chemical structures of molecules, the molecular spacer arms are 0.33 nm[1], 1.35 nm[2], and 2-4 nm[3,4] in length for APTES, NHS-biotin, streptavidin, respectively. Therefore, the total thickness can be approximately evaluated to be between 3.68 nm and 5.68 nm. The purpose of the evaluation of thickness is to confirm that all the gain molecules were within the reach of the evanescent wave of the optical fibre microcavities, about 100 nm according to the numerical simulation (Fig. S4).

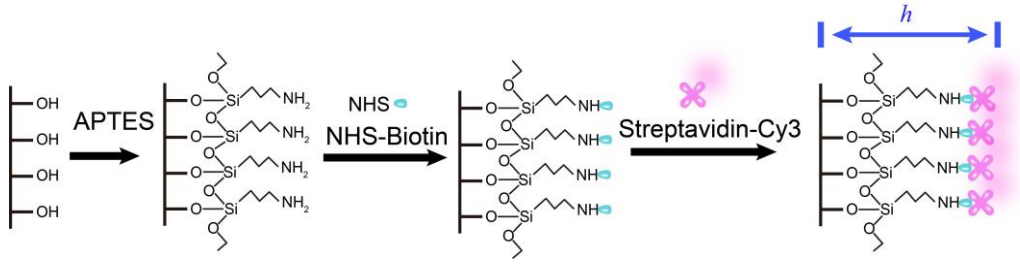

Figure S1. Illustration of the surface modification for the submonolayer biolaser based on the biotin-streptavidin conjugation. *h* denotes the distance from the Cy3 molecules to the surface of the silica optical fibre.

2. Q-factor measurement of the optical fibre microcavities

The bare optical fibres were immersed in PBS, and the fibre taper coupling method illustrated in Fig. S2a was employed for Q-factor measurements. The detailed procedure is described in Methods. We randomly selected 22 different locations on the optical fibre to test. A typical transmission spectrum is shown in Fig. S2b. The average Q-factor of the optical fibre microcavities was measured to be 1.2×10^6 with a coefficient of variation of 16 % (Fig. S2c).

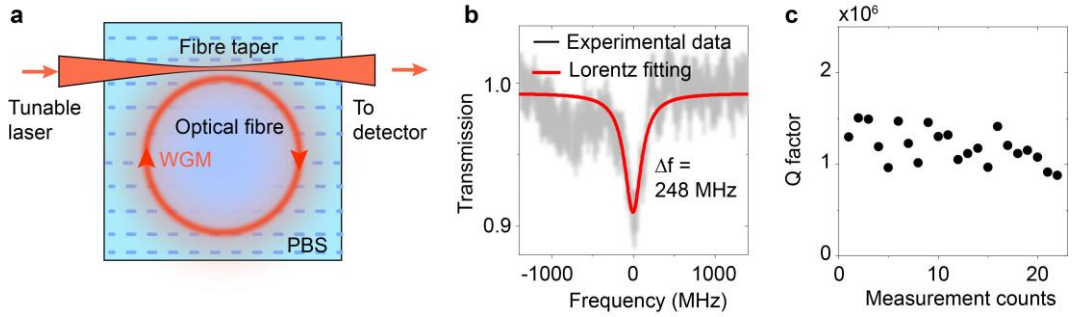

Figure S2. a, Schematic illustration of the experimental setup for Q-factor tests. **b,** A typical resonant dip in the frequency domain. **c,** The measured Q-factor of the microcavities at different locations of an optical fibre.

3. Laser threshold

The laser threshold of the submonolayer biolaser is strongly dependent on the surface density of gain molecules, which can be controlled with biotin concentrations. The typical laser threshold curves with different biotin concentrations are illustrated in Fig. S3.

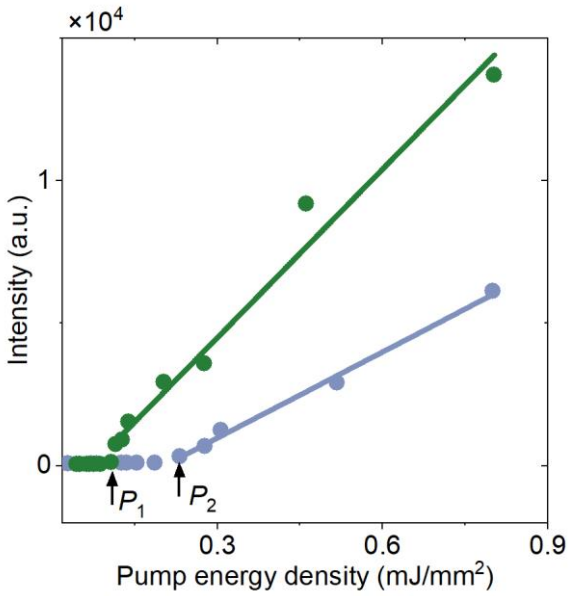

Figure S3. The threshold curves with biotin concentrations of 400 μM (green) and 200 μM (blue), respectively. Laser thresholds: P_1 = 0.09 mJ/mm^2; P_2 = 0.22 mJ/mm^2.

4. Numerical simulation of optical resonance in the fibre microcavity

The numerical simulations show the optical resonance at specific resonant frequencies in the optical fibre microcavity (Fig. S4a). The enlargement of the intensity distribution in Fig. S4b indicates a penetration depth of about 100 nm of the evanescent wave (inset of Fig. S4b).

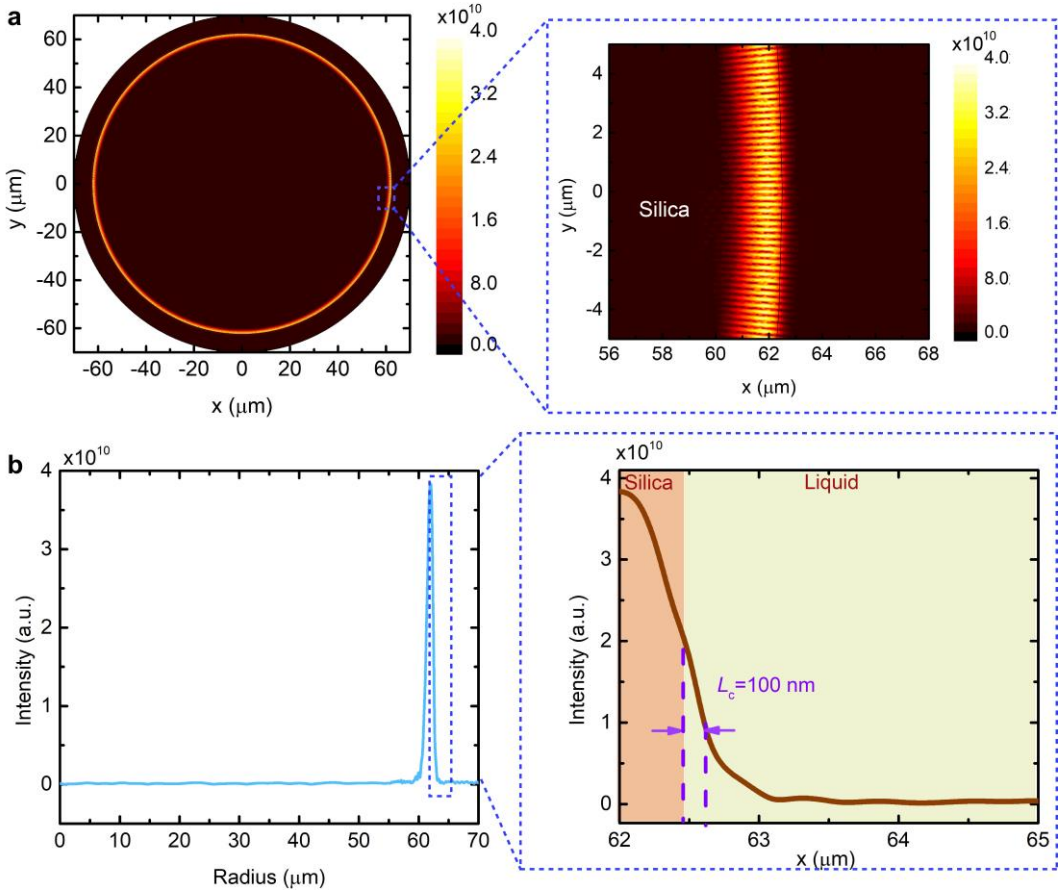

Figure S4. a, Numerical simulation of intensity distribution on the cross-section of the optical fibre. Inset, enlargement of the region in the dashed box. **b,** The radial intensity distribution with a resonant peak, data was derived from **a**. Inset, enlargement of the boxed region.

5. Analysis of the surface density of Cy3 molecules

The threshold condition for a four-level laser system can be expressed as[5]

$$\eta D_1 \sigma_e(\lambda) = \eta \sigma_a(\lambda) D_0 + \frac{2\pi n}{\lambda_L Q}. \quad (1)$$

Here, η = 2.67% is the fraction of energy that interacts with the gain molecules, which can be calculated in Fig. S4. D_0 and D_1 are the density of dye molecules in the ground state and the lowest excited singlet state, respectively. σ_e and σ_a represent the emission and absorption cross-sections, respectively. λ_L denotes the laser wavelength and Q stands for the Q-factor. n is the effective refractive index of the exciting mode of the fibre ring resonator. Thus, the fraction of molecules in the excited state can be given by

$$\gamma = \frac{D_1}{D_0 + D_1} = \frac{\sigma_a(\lambda)}{\sigma_e(\lambda)} \left(1 + \frac{2\pi n}{\lambda_L D \eta Q \sigma_a(\lambda)}\right). \quad (2)$$

Here, $D = D_0 + D_1$ denotes the density of total gain molecules. According to the rate equation for a four-level laser system, γ can also be approximated as[6]

$$\gamma = \frac{w_p \tau_{rad}}{1 + w_p \tau_{rad}} \quad (3)$$

Here, $w_p = I_{th}\sigma_a / E_0 \Delta t$ is the normalized pump intensity. I_{th} is the laser threshold. $E_0 = hc/\lambda_p$ is the photon energy of the pump. Δt is the pulse width of the pump laser. τ_{rad} is the lifetime of the excited state.

According to the conclusions in Figs. S1 and S4, all the Cy3 molecules conjugated on the optical fibre are located within the reach of the evanescent field and can thus be involved in the optical resonance. Therefore, once the laser threshold is measured, N can be numerically calculated by using Supplementary Eqs. (2) and (3). The surface density of gain molecules is calculated using $S=D*d$, with d =100 nm denoting the penetration depth (Fig. S4). We calculated the dependence of I_{th} on S with various Q-factors and the results are illustrated in Fig. S5, through which we can estimate the surface density of gain molecules on fibre by the given threshold.

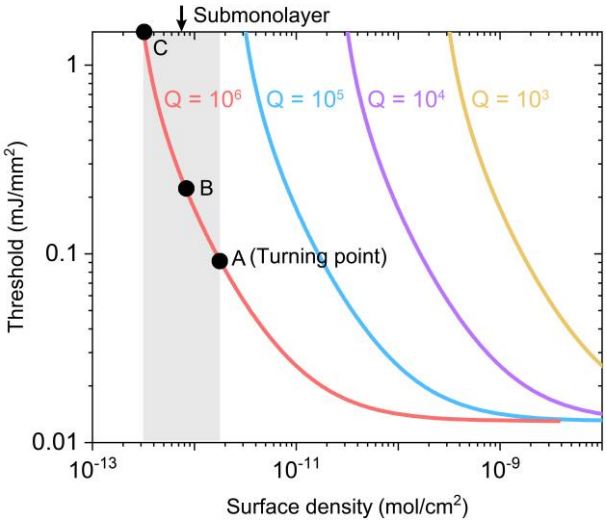

Figure S5 Numerical results of the laser threshold as a function of the surface density of Cy3 molecules. The grey area denotes the submonolayer biolaser.

6. Characterization of laser emission

6.1 Reproducibility of laser threshold

The frequency histogram of laser threshold was illustrated in Fig. S6, indicating an average threshold of 0.6 mJ/mm^2. Comparing with the threshold given in Fig. S3, the higher threshold is caused by a lower NHS-biotin concentration.

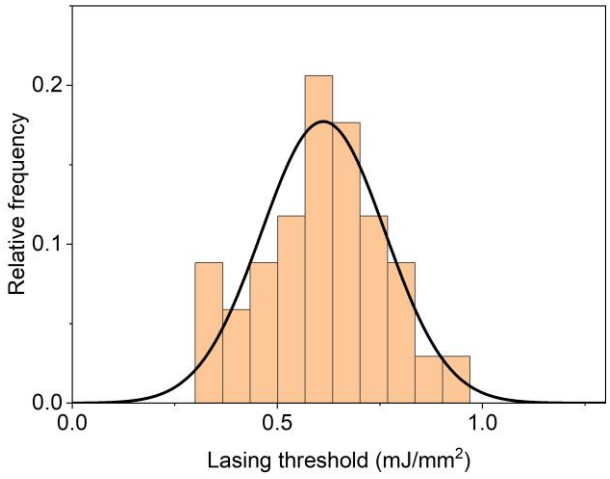

Figure S6. Frequency histogram of 34 submonolayer biolasers. These submonolayer biolasers were fabricated using 100 μM NHS-biotin.

6.2 Statistical distribution of laser emission

A batch of 736 biolasers was tested to investigate the statistical distribution of the laser intensity (Fig. S7). The relative laser intensity in decibels of each test was calculated, which formed a normal distribution. The characteristics of the statistical distribution were analyzed and the mean was selected as a sensor indicator.

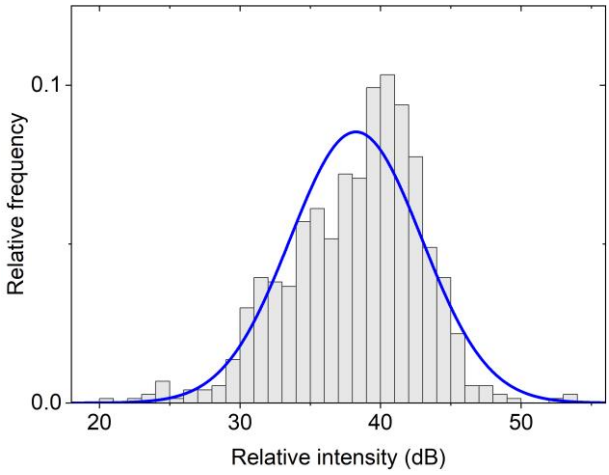

Figure S7. Frequency histogram of relative intensity. Data are extracted from 736 submonolayer biolasers.

7. Ultrahigh sensitivity of the submonolayer biolasers

7.1 Theoretical model for sensitivity analysis

The laser intensity can be written as[6]

$$I_{laser} = A\left(\frac{I_{pump}}{I_{th}} - 1\right). \tag{4}$$

Here, I_{pump} is the pump intensity and I_{th} is the laser threshold. A is a constant.

Combining with Supplementary Eqs. (3) to (4), we derive that

$$I_{laser} = A\left[\frac{I_{pump}\sigma_a\tau_{rad}}{E_0\Delta t}\left(\frac{1}{\gamma} - 1\right) - 1\right]. \tag{5}$$

This equation shows the dependence of the laser intensity on γ. Then we can calculate the laser emission as a function of the surface density (S).

In immunoassay, the number of gain molecules is proportional to the number of conjugated antigen molecules. The sensitivity of the laser-based sensor to the antigen on fibre can be defined as

$$\frac{dI_{laser}}{dS} = \frac{dI_{laser}}{d\gamma} \cdot \frac{d\gamma}{dD} \cdot \frac{dD}{dS}. \tag{6}$$

Here,

$$\frac{dI_{laser}}{d\gamma} = -A \cdot \frac{I_{pump}\tau_{rad}\sigma_a}{E_0\Delta t} \cdot \frac{1}{\gamma^2}, \tag{7}$$

$$\frac{d\gamma}{dD} = -\frac{2\pi n}{\sigma_e \lambda_L \eta Q} \cdot \left(\frac{S}{d}\right)^2, \tag{8}$$

and

$$\frac{dD}{dS} = \frac{1}{d} \tag{9}$$

According to the analysis above, theoretical calculation of the sensitivity as a function of Cy3 surface density was shown in Fig. 2c. The results indicate an increase in sensitivity with a lower surface density and an ultrahigh sensitivity can be achieved when the surface density decreases to the threshold density.

Comparatively, in the fluorescence tests, the emission intensity can be written as

$$I_{FL} = B \cdot S \cdot I_{pump} \tag{10}$$

Here, B is a constant. The sensitivity of the fluorescence-based sensor can be defined as

$$\frac{dI_{FL}}{dS} = B \cdot I_{pump} \tag{11}$$

Therefore, the sensitivity of the fluorescence-based sensor remains independent of the molecular surface density.

7.2 Exploring the ultimate sensitivity of the submonolayer biolasers

The ultimate sensitivity can be achieved the surface density of gain molecules close to the threshold density (~ 3.2 $\times 10^{-13}$ mol/cm^2, Point C in Fig. S5). In this case, a dramatic decrease in lasing intensity can be observed when the avidin concentration reaches 1fM and the laser extinguished with 10 fM avidin. The typical emission spectra with various avidin concentrations are illustrated in Fig. S8.

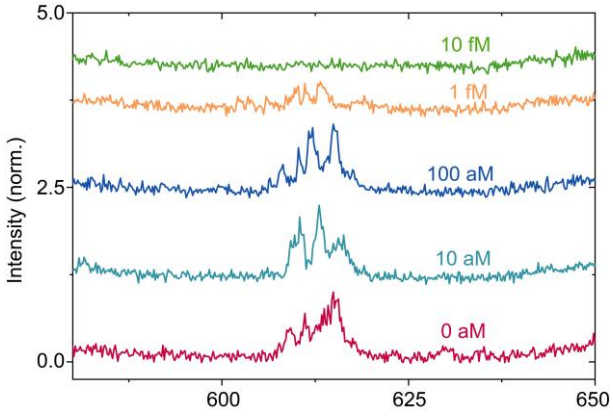

Figure S8. Spectral evolution of submonolayer biolaser with different concentrations of avidin.

8. Alpha-synuclein detection in buffer

We tested the performance of the submonolayer biolasers in buffer solution. The detailed procedure can be found in Methods. The statistical distribution continuously shifts toward right with a higher α-syn concentration (Fig. S9).

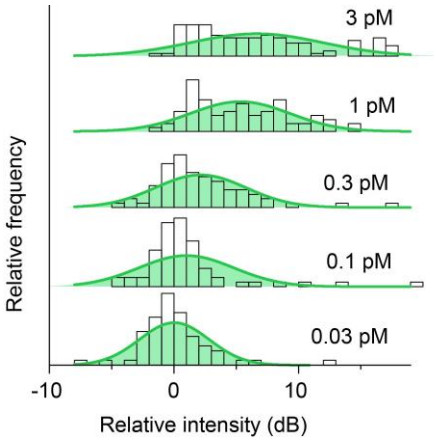

Figure S9. Statistical distribution of the relative intensity at different α-syn concentrations in buffer.

9. Experimental setup

The experiment setup is illustrated in Fig. S10. The optical fibre was fixed on a motorized stage and the position of the optical fibre moves in the fibre axis direction with a step of 250 μm, thus enabling a quick scanning of the pump strip along the optical fibre. More details of the experimental setup can be found in Methods.

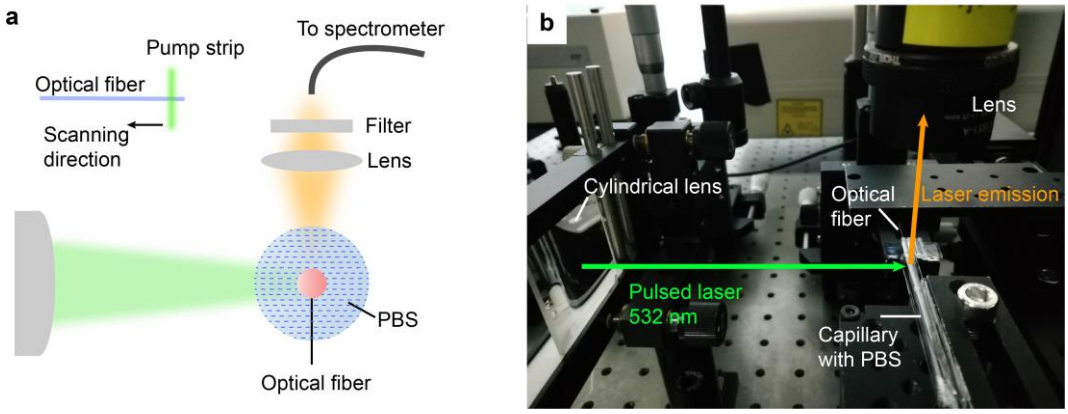

Figure S10. Conceptual illustration (**a**) and the photo (**b**) of the experimental setup.

References

1 Yang, S.-q. *et al.* Effect of reaction temperature on grafting of γ-aminopropyl triethoxysilane (APTES) onto kaolinite. *Appl. Clay Sci.* **62**, 8-14, (2012).

2 Cohn, J. V., Alkhalil, A., Wagner, M. A., Rajapandi, T. & Desai, S. A. Extracellular lysines on the plasmodial surface anion channel involved in Na+ exclusion. *Mol. Biochem. Parasitol.* **132**, 27-34, (2003).

3 Ding, Z., Fong, R. B., Long, C. J., Stayton, P. S. & Hoffman, A. S. Size-dependent control of the binding of biotinylated proteins to streptavidin using a polymer shield. *Nature* **411**, 59-62, (2001).

4 Weber, P. C., Ohlendorf, D. H., Wendoloski, J. & Salemme, F. Structural origins of high-affinity biotin binding to streptavidin. *Science* **243**, 85-88, (1989).

5 Moon, H.-J., Chough, Y.-T. & An, K. Cylindrical microcavity laser based on the evanescent-wave-coupled gain. *Phys. Rev. Lett.* **85**, 3161, (2000).

6 Siegman, A. E. *Lasers* (University science books, 1986).